IEEE Access
Multidisciplinary | Rapid Review | Open Access Journal

Received April 3, 2020, accepted April 12, 2020, date of publication April 15, 2020, date of current version April 30, 2020.

Digital Object Identifier 10.1109/ACCESS.2020.2988096

Analytical Design of Dual-Band Negative Group Delay Circuit With Multi-Coupled Lines

XIANG ZHOU[1], (Member, IEEE), BINHONG LI[2], NINGDONG LI[3], BLAISE RAVELO[3], (Member, IEEE), XIAOFENG HU[4], QIZHENG JI[5], FAYU WAN[3], (Member, IEEE), AND GLAUCO FONTGALLAND[6], (Senior Member, IEEE)

[1]School of Mechanical Engineering, Southeast University, Nanjing 210096, China
[2]Key Laboratory of Silicon Device Technology, Chinese Academy of Sciences, Beijing 100029, China
[3]School of Electronic and Information Engineering, Nanjing University of Information Science and Technology, Nanjing 210044, China
[4]National Key Laboratory of Electromagnetic Environment Effect, Army Engineering University of PLA, Shijiazhuang 050003, China
[5]Beijing Orient Institute of Measurement and Test, Beijing 100094, China
[6]Applied Electromagnetic and Microwave Laboratory, Federal University of Campina Grande, Campina Grande 58429, Brazil

Corresponding author: Fayu Wan (fayu.wan@nuist.edu.cn)

This work was supported in part by the NSFC under Grant 61971230 and Grant 61601233, in part by the Jiangsu Distinguished Professor program and Six Major Talents Summit of Jiangsu Province under Grant 2019-DZXX-022, in part by the Postgraduate Research and Practice Innovation Program of Jiangsu Province under Grant SJKY19_0974, and in part by the Priority Academic Program Development of Jiangsu Higher Education Institutions (PAPD) fund.

ABSTRACT This paper develops an innovative design method of a multi-coupled line (CL) topology of low-loss dual band negative group delay (NGD) circuit. The proposed is conceived using three transmission lines (TLs) with different length in which integrate two couplers. The three traveling paths are designed to generate the dual-band NGD effect, where the CLs allow lowering the signal attenuation. The NGD circuit S-parameter model as a function of the TLs physical lengths and coupling coefficient are established. To validate the NGD circuit proof-of-concept, it is fabricated and measured. The NGD values of approximately –4.06 ns and –3.83 ns are measured at center frequencies of 2.43 GHz and 3.02 GHz, respectively. The measured transmission coefficient is better than −2.9 dB and the measured reflection one is better than −12 dB into the NGD band. The measurement results of the NGD circuit are in good agreement with the simulations results.

INDEX TERMS Low-loss, dual-band, negative group delay (NGD), S-parameter model, coupled lines.

I. INTRODUCTION

Theoretical analysis and experimental researches in the microwave field demonstrated that the existence of negative group delay (NGD) phenomenon was reasonable at certain passive circuits [1]–[5]. This abnormal physical phenomenon can be proven to occur around the resonance frequency of the absorptive media.

The NGD special effect with respect to time advancement without violation of causality and relativity [1], [6] usually plays an important role in designing high performance microwave phase shifters [7]–[9] or delay equalizers [10]–[12], feedforward and feedback amplifiers [13]–[15], antennas [16]–[19], and non-Foster elements [20]–[23]. For example, to resolve signal distortion caused by delay fluctuations in wireless communication systems, an equalization solution to the delay compensation and signal recovery was introduced in [10]. In addition, further novel methods of higher performance microwave circuits based on the NGD circuit for designing feedforward [13], [14] and feedback amplifier [15] topologies were developed. These innovative NGD circuits were designed with competitive size reduction, enhanced efficiency, and significant improvement on the bandwidth, as introduced in [13]–[15]. As stressed in [16] and [19], non-foster elements synthesized by NGD networks are employed to overcome beam squinting of series-fed antenna arrays. Furthermore, in order to exhibit unconditional stability, a novel type of non-Foster element by using a microwave transversal-filter-based NGD circuit is presented in [21].

In recent years, with the orthodox development of its research and exploration, the NGD circuits can be divided into two categories: active and passive NGD circuits. The NGD functional characteristic can be implemented easily by

The associate editor coordinating the review of this manuscript and approving it for publication was Feng Lin.

using some simple active microwave circuits that initially depended only on passive lumped elements, such as resistor R, inductor L, and capacitor C [24]–[26]. The low-pass, high-pass, bandpass, and stop-band NGD circuit cells were designed to understand the basic NGD properties and synthesis methodology in [26]. Most of these existing active NGD microwave circuits based on the use of low noise amplifiers (LNAs) and field effect transistors (FETs) associated with lumped RLC resonant networks have recently been proposed and developed [27]–[30]. It was found that these active NGD circuits would unavoidably suffer from design inflexibility restrictions on lumped components as well as increasing design difficulties in the microwave band.

To overcome these limitations, some topologies of the passive NGD circuits implemented by distributed elements such as transmission line (TL) and coupled line (CL) were developed [31]–[34]. In [31] and [34], the passive NGD circuits have unavoidable large signal attenuation in the desired NGD bandwidth. To obtain low signal attenuation, two short-circuited coupled lines with high characteristic impedance and small coupling coefficient. The circuits' losses in the case of types-I and type-II NGD networks were decreased to 7.43 dB and 9.23 dB, respectively, [35]. Furthermore, a general-purpose gain amplifier can be used to compensate signal attenuation of the passive NGD networks [16], [36]. However, it can increase the out-of-band noise thus making the circuit more complicated.

Compared to single-band NGD microwave devices [16], [31]–[36], the design of dual-band NGD circuits [37]–[39] remains a challenging task, notably for RF non-specialist and microwave design engineers. Similarly to most of RF and microwave functions (such as filters, phase shifters, amplifiers, power combiners/dividers), the NGD functions should be susceptible to operate in different frequency bands. However, so far, few studies focused on the design of dual-band NGD circuits are available. As reported in the literature [37], a single-band reflection type NGD circuit composed of two short stubs are employed to achieve two separate frequency bands, where the attenuation has exceeded 30 dB. Among the existing dual-band NGD circuit, one can cite a miniaturized dual-band NGD passive device proposed in [38]. The design of this miniature circuit was carried out by utilizing dual-plane U-shaped defected structures (attenuation $>$ 35 dB). An 18 dB attenuation was obtained using a compact dual-band NGD circuit composed of an open-circuited TL and two resistors connected by two TLs, as proposed in [39]. The drawbacks in the design of NGD circuit applications is the severe signal attenuation, which profoundly affects the NGD performances and limit their possibilities. Therefore, it becomes important to design low-loss dual-band NGD circuit. An active dual band is presented in [40] and an arbitrary frequency ratio dual band is presented in [41].

In this paper, a topology of passive circuit based on fully distributed elements is proposed. The design does not require any external RF amplifier. The proposed NGD topology consists of two identical coupled lines (CLs) and three different transmission lines' length (TLs).

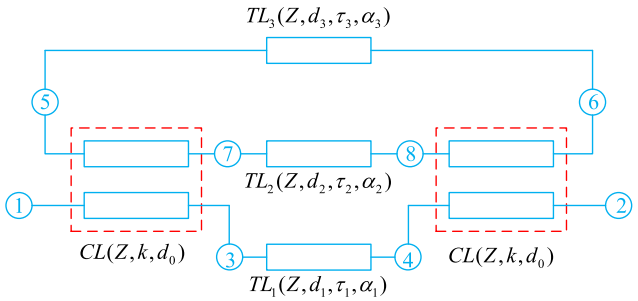

FIGURE 1. Multi-CL based topology under study.

The paper is mainly organized in four different sections. In Section II, the topological analysis and S-parameter model are introduced. Based on the input and output wave powers analysis, the microwave circuit theory established from S-parameters model of the innovative NGD topology is developed. In Section III, the analytical expression of the group delay derived from transmission coefficient is presented. The NGD analysis as a function of frequencies related to the constituting NGD topology TL parameters is also given. To verify the feasibility of the design, the investigation of NGD circuit prototypes are described in Section IV. Afterwards, the theoretical, simulated, and measured results are compared and discussed. Finally, this paper is ended by a conclusion in Section V.

II. TOPOLOGICAL ANALYSIS AND S-PARAMETER MODEL

This section mainly describes the theoretical analysis of the multi-coupled line NGD topology. After description of the topological structure, the NGD circuit design is conceived from the combination of the CL and TL theories, based on the S-parameter model. The group delay analytical expression is also provided. Then, the NGD analysis will be introduced.

A. TOPOLOGICAL ANALYSIS

Fig. 1 shows the topology of the proposed NGD circuit under study. This circuit topology behaves as a two-port network without using any lossy lumped elements. The circuit consists of two identical CLs with ① -③-⑤-⑦ and ② -④-⑥-⑧ connection ports. As depicted in Fig. 1, the left CL port ① and the right CL port ② serve as main input and output for overall NGD cell, respectively. Furthermore, the left CL port ③ (resp. ⑦, ⑤) and the right CL port ④ (resp. ⑧, ⑥) are interconnected through a lossy TL_1 (resp. TL_2, TL_3) where the characteristic impedance is $Z = 50\ \Omega$, d_1 (resp. d_2, d_3) is the physical length, τ_1 (resp. τ_2, τ_3) is the delay, and α_1(resp. α_2, α_3) is the attenuation loss.

It is worth emphasizing that the TL_m length d_m and the CL length d_0 have the following relationship:

$$\begin{cases} d_1 = 2d_0 \\ d_2 = 6d_0 \\ d_3 = 10d_0. \end{cases} \tag{1}$$

Therefore, the TL_m delay, τ_m, and attenuation loss, a_m, can be expressed as

$$\begin{cases} \tau_1 = 2\tau_0 \\ \tau_2 = 6\tau_0 \\ \tau_3 = 10\tau_0 \end{cases} \tag{2}$$

and

$$\begin{cases} \alpha_1 = \alpha_0^2 \\ \alpha_2 = \alpha_0^6 \\ \alpha_3 = \alpha_0^{10}. \end{cases} \tag{3}$$

The parameters τ_0 and α_0 represent the delay and attenuation loss of a microstrip line with a length of d_0, respectively. In addition, a_m and b_m ($m = \{1, \ldots, 8\}$) represent the input and output wave powers.

B. S-PARAMETER MODEL FROM THE TL AND CL COMBINED THEORIES

The main purpose of the present theoretical recall is to establish the group delay analytical expression of the topology introduced in Fig. 1. To do this, a S-matrix model is needed. The expected S-matrix will be determined by the mean of the TL and CL combined theories.

1) RECALL ON CL THEORY

According to the microwave theory, the CL S-matrix can be expressed as [32]:

$$[S]_{CL} = \begin{bmatrix} 0 & k_1 & k & 0 \\ k_1 & 0 & 0 & k \\ k & 0 & 0 & k_1 \\ 0 & k & k_1 & 0 \end{bmatrix}, \tag{4}$$

where k is the CL coupling coefficient and:

$$k_1 = -j\sqrt{1-k^2}, \tag{5}$$

and $j^2 = -1$. Here, the coupling coefficient k must satisfy the condition $0 < k < 1$. In the present study, the CL propagation delay is assumed to be negligible.

2) RECALL ON TL THEORY

One assumes that the TLs is lossy, matched, and can be constituted by the topology shown in Fig. 1. Let us denote τ_m the propagation delay and a_m the attenuation loss of the elementary transmission line, TL_m with $m = \{1, 2, 3\}$. According to the TL theory, the TL_m S- matrices are given by

$$[S]_{TL_m} = \begin{bmatrix} S_{11_{TL_m}} & S_{12_{TL_m}} \\ S_{21_{TL_m}} & S_{22_{TL_m}} \end{bmatrix}, \tag{6}$$

with

$$\begin{cases} S_{11_{TL_m}} = S_{22_{TL_m}} = 0 \\ S_{12_{TL_m}} = S_{21_{TL_m}} = x_m = \alpha_m e^{-j\omega\tau_m}. \end{cases} \tag{7}$$

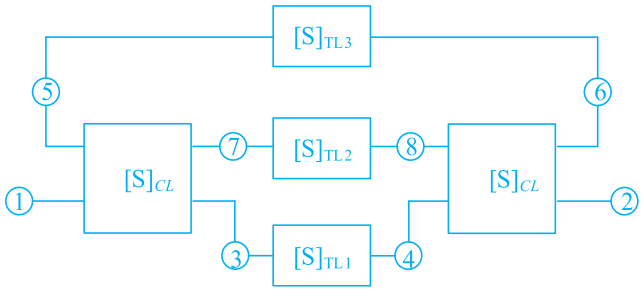

FIGURE 2. Block diagram equivalent to the NGD topology under study.

C. S-PARAMETER MODEL OF THE NGD TOPOLOGY

The block diagram equivalent of our topology can be seen in Fig. 2. First, according to the CL configuration of the diagram shown in Fig. 2, the CL S-matrix are analytically interacted with the wave powers by the relationships

$$\begin{bmatrix} b_1 \\ b_3 \\ b_5 \\ b_5 \end{bmatrix} = [S]_{CL} \times \begin{bmatrix} a_1 \\ a_3 \\ a_5 \\ a_7 \end{bmatrix}, \tag{8}$$

and

$$\begin{bmatrix} b_2 \\ b_4 \\ b_6 \\ b_8 \end{bmatrix} = [S]_{CL} \times \begin{bmatrix} a_2 \\ a_4 \\ a_6 \\ a_8 \end{bmatrix}. \tag{9}$$

In addition, the three TL S-parameters are linked to the TL wave powers access port by the following matrix relation:

$$\begin{bmatrix} a_3 \\ a_4 \end{bmatrix} = \begin{bmatrix} S_{11TL_1}(j\omega) & S_{12TL_1}(j\omega) \\ S_{21TL_1}(j\omega) & S_{22TL_1}(j\omega) \end{bmatrix} \times \begin{bmatrix} b_3 \\ b_4 \end{bmatrix}, \tag{10}$$

$$\begin{bmatrix} a_7 \\ a_8 \end{bmatrix} = \begin{bmatrix} S_{11TL_2}(j\omega) & S_{12TL_2}(j\omega) \\ S_{21TL_2}(j\omega) & S_{22TL_2}(j\omega) \end{bmatrix} \times \begin{bmatrix} b_7 \\ b_8 \end{bmatrix}, \tag{11}$$

$$\begin{bmatrix} a_5 \\ a_6 \end{bmatrix} = \begin{bmatrix} S_{11TL_3}(j\omega) & S_{12TL_3}(j\omega) \\ S_{21TL_3}(j\omega) & S_{22TL_3}(j\omega) \end{bmatrix} \times \begin{bmatrix} b_5 \\ b_6 \end{bmatrix}. \tag{12}$$

Substantially, we have:

$$\begin{cases} a_3 = \alpha_1 e^{-j\omega\tau_1} b_4 \\ a_4 = \alpha_1 e^{-j\omega\tau_1} b_3 \\ a_7 = \alpha_2 e^{-j\omega\tau_2} b_8 \\ a_8 = \alpha_2 e^{-j\omega\tau_2} b_7 \\ a_5 = \alpha_3 e^{-j\omega\tau_3} b_6 \\ a_6 = \alpha_3 e^{-j\omega\tau_3} b_5. \end{cases} \tag{13}$$

According to the S-parameter theory, this two-port NGD network main access wave powers can be defined by the matrix relation

$$\begin{bmatrix} b_1(j\omega) \\ b_2(j\omega) \end{bmatrix} = \begin{bmatrix} S_{11}(j\omega) & S_{12}(j\omega) \\ S_{21}(j\omega) & S_{22}(j\omega) \end{bmatrix} \times \begin{bmatrix} a_1(j\omega) \\ a_2(j\omega) \end{bmatrix}. \tag{14}$$

It can be seen from matrix equation (14) that the S-parameter model of the entire circuit can be obtained by calculating the output wave powers b_1 and b_2, and the input wave power a_1 and a_2. By combining equations (2)-(14),

one has the frequency dependent reflection and transmission coefficients of the NGD circuit previously introduced in (14) and rewritten as:

$$\begin{cases} S_{11}(j\omega) = S_{22}(j\omega) = 0 \\ S_{21}(j\omega) = S_{12}(j\omega) = \dfrac{k_1^2 x_1 + k^2 x_3 - x_1 x_2 x_3}{1 - k_1^2 x_2 x_3 - k^2 x_1 x_2}. \end{cases} \tag{15}$$

Consequently, the S-parameter element magnitude and group delay expressions will be analytically explored in the next section.

III. NGD THEORY OF THE MULTI-COUPLED LINE NGD TOPOLOGY

Based on the previously expressed S-parameter model, the NGD theory of the multi-CL based topology will be established in this section. Before the NGD analysis, the magnitude and phase of the transmission coefficient will be presented.

A. TRANSMISSION COEFFICIENT MAGNITUDE AND PHASE

The magnitude $S_{21}(\omega) = |S_{21}(j\omega)|$ of the transmission coefficient formulated in (15) is given by

$$S_{21}(\omega) = \sqrt{\frac{R_1^2(\omega) + R_2^2(\omega)}{R_3^2(\omega) + R_4^2(\omega)}}, \tag{16}$$

with

$$\begin{cases} R_1(\omega) = \left\{ \begin{matrix} k_1^2\alpha_1 \cos(\omega\tau_1) + k^2\alpha_3 \cos(\omega\tau_3) \\ -\alpha_1\alpha_2\alpha_3 \cos[\omega(\tau_1+\tau_2+\tau_3)] \end{matrix} \right\} \\ R_2(\omega) = -\left\{ \begin{matrix} k_1^2\alpha_1 \sin(\omega\tau_1) + k^2\alpha_3 \sin(\omega\tau_3) \\ -\alpha_1\alpha_2\alpha_3 \sin[\omega(\tau_1+\tau_2+\tau_3)] \end{matrix} \right\} \\ R_3(\omega) = \left\{ \begin{matrix} 1 - k_1^2\alpha_2\alpha_3 \cos[\omega(\tau_2+\tau_3)] \\ -k^2\alpha_1\alpha_2 \cos[\omega(\tau_1+\tau_2)] \end{matrix} \right\} \\ R_4(\omega) = \left\{ \begin{matrix} k_1^2\alpha_2\alpha_3 \sin[\omega(\tau_2+\tau_3)] \\ +k^2\alpha_1\alpha_2 \sin[\omega(\tau_1+\tau_2)] \end{matrix} \right\}. \end{cases} \tag{17}$$

The proposed NGD topology transmission phase $\varphi(\omega) = \arg[S_{21}(j\omega)]$, can also be deduced from transmission coefficient expression previously introduced in (16). The phase detailed expression is written as

$$\varphi(\omega) = \varphi_n(\omega) - \varphi_d(\omega), \tag{18}$$

with

$$\varphi_n(\omega) = \arctan\frac{R_2(\omega)}{R_1(\omega)}, \tag{19}$$

and

$$\varphi_d(\omega) = \arctan\frac{R_4(\omega)}{R_3(\omega)}. \tag{20}$$

B. GROUP DELAY FREQUENCY-DEPENDENT EXPRESSION

The expected group delay calculated from previously expressed transmission phase (18) is defined by

$$\tau(\omega) = -\frac{\partial\varphi(\omega)}{\partial\omega} = \tau_d(\omega) - \tau_n(\omega), \tag{21}$$

with

$$\begin{cases} \tau_d(\omega) = -\dfrac{\partial\varphi_d(\omega)}{\partial\omega} \\ \tau_n(\omega) = -\dfrac{\partial\varphi_n(\omega)}{\partial\omega}. \end{cases} \tag{22}$$

Knowing the quantities expressed previously in (21) and (22), one has

$$\tau_d(\omega) = \frac{R_4'(\omega)R_3(\omega) - R_3'(\omega)R_4(\omega)}{R_3^2(\omega) + R_4^2(\omega)}, \tag{23}$$

with

$$\begin{cases} R_3' = \left\{ \begin{matrix} (\tau_2+\tau_3)k_1^2\alpha_2\alpha_3 \sin[\omega(\tau_2+\tau_3)] \\ +(\tau_1+\tau_2)k^2\alpha_1\alpha_2 \sin[\omega(\tau_1+\tau_2)] \end{matrix} \right\} \\ R_4' = \left\{ \begin{matrix} (\tau_2+\tau_3)k_1^2\alpha_2\alpha_3 \cos[\omega(\tau_2+\tau_3)] \\ +(\tau_1+\tau_2)k^2\alpha_1\alpha_2 \cos[\omega(\tau_1+\tau_2)] \end{matrix} \right\}, \end{cases} \tag{24}$$

and

$$\tau_n(\omega) = \frac{R_2'(\omega)R_1(\omega) - R_2(\omega)R_1'(\omega)}{R_1^2(\omega) + R_2^2(\omega)}, \tag{25}$$

with

$$\begin{cases} R_1'(\omega) = \left\{ \begin{matrix} -\tau_1 k_1^2\alpha_1 \sin(\omega\tau_1) - \tau_3 k^2\alpha_3 \sin(\omega\tau_3) \\ +(\tau_1+\tau_2+\tau_3)\alpha_1\alpha_2\alpha_3 \sin[\omega(\tau_1+\tau_2+\tau_3)] \end{matrix} \right\} \\ R_2'(\omega) = -\left\{ \begin{matrix} \tau_1 k_1^2\alpha_1 \cos(\omega\tau_1) + \tau_3 k^2\alpha_3 \cos(\omega\tau_3) \\ -(\tau_1+\tau_2+\tau_3)\alpha_1\alpha_2\alpha_3 \cos[\omega(\tau_1+\tau_2+\tau_3)] \end{matrix} \right\}. \end{cases} \tag{26}$$

To validate this multi-CL NGD theory, a circuit is designed to achieve a low loss dual-band NGD circuit. To materialize the feasibility of the NGD function, the next section will present the validation results from simulations and measurements.

IV. SIMULATED AND MEASURED BEHAVIOR OF A DUAL-BAND NGD TOPOLOGY

The present section discusses the validations of the developed NGD topology. The validation is originally focused on the proof-of-concept (POC) showing dual-band NGD behavior by means of S-parameter theory, simulations, and measurements. The simulations are carried out with the HFSS simulation tool while the measurements are realized using a Vector Network Analyzer (VNA).

A. POC DESIGN DESCRIPTION

Figs. 3 presents the design of the NGD POC. The NGD layout realized in the HFSS 3-D EM environment is shown in Fig. 3(a) and the optimized final physical dimensions are presented in Table 1. The picture of the fabricated NGD circuit is shown in Fig. 3(b).

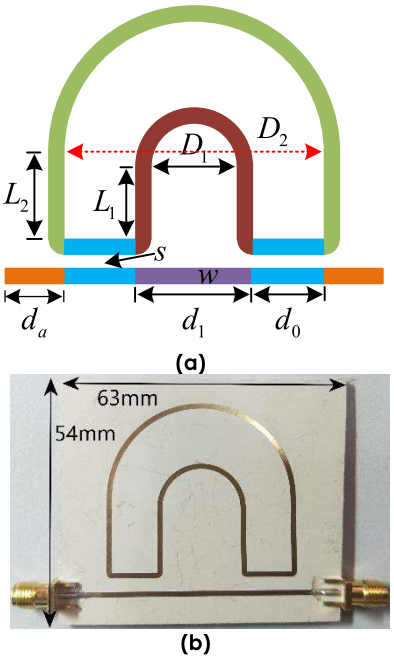

FIGURE 3. NGD circuit prototype: (a) layout and (b) prototype.

The overall size of the circuit is 54 mm × 63 mm. The NGD prototype was built as a microstrip planar circuit, on the Rogers 3210 substrate. The TLs and CLs electrical and physical parameters are shown in Table 1. The curved TL_2 and TL_3 lines are designed to reduce the circuit size and generate a simple layout. It is noteworthy that to design the dual-band NGD circuits based on the topology under study with required arbitrary frequencies, we can proceed with:

- The calculations of delays τ_1, τ_2 and τ_3 by controlling the physical lengths d_1, (L_1, D_1) and (L_2, D_2), respectively of the structure shown in Fig. 3 in function of the required frequencies,
- To control the frequency f_1, we can modify the physical length d_1,
- And acting as a distributed microwave circuit depending on TL design, the ratio between the dual NGD center frequencies f_2/f_1, can be chosen as the ratio between the fundamental and harmonic frequencies.

To confirm the theoretical hypothesis presented in Subsection II-B, it is noteworthy that the CL propagation delay associated to 10.56 mm is approximately 0.18 ns. This value can be neglected when compared to NGD absolute value, which is approximately −4 ns.

B. PARAMETRIC ANALYSES OF d_0 AND s

Parametric analyses with respect to the physical length d_0 and coupling space s, have been conducted. The parametric analyses enable to explain more explicitly the length and coupling coefficient effects onto the NGD function. Two cases of S-parameter parametric simulations are carried out with HFSS®simulator from ANSYS®by changing d_0 and s.

TABLE 1. The electrical and physical parameters of NGD POC.

Components	*Description*	*Parameter*	*Value*
Dielectric substrate	Material	Rogers 3210	-
	Relative permittivity	ε_r	10.2
	Loss tangent	tan(δ)	0.0027
	Thickness	h	1.27 mm
Metallization	Material	Copper (Cu)	-
	Thickness	t	35 µm
	Conductivity	σ	58 MS/m
TL_1	Total length	d_1	21.12 mm
	width	w	1.18 mm
	attenuation loss	α_1	-0.05 dB
	delay	τ_1	0.184 ns
TL_2	Total length	d_2	63.36 mm
	width	w	1.18 mm
	attenuation loss	α_2	-0.15 dB
	delay	τ_2	0.552 ns
	partial length	L_1	15.092 mm
	diameter	D_1	18.76 mm
TL_3	Total length	d_3	105.6 mm
	width	w	1.18 mm
	attenuation loss	α_3	-0.25 dB
	delay	τ_3	0.92 ns
	partial length	L_2	17.771 mm
	diameter	D_2	42.24 mm
CL	length	d_0	10.56 mm
	width	w	1.18 mm
	Interspace	s	3 mm
	Coupling coefficient	k	-25.64 dB
Access line	length	d_a	10 mm
	width	w	1.18 m

1) PARAMETRIC ANALYSIS OF THE LENGTH d_0

The current parametric analysis is mainly to explore the effect of physical length d_0 on NGD function. As indicated in Section II.A, the length of CLs and TLs are all related to d_0. By increasing d_0 will increase the length of CLs and the three TLs. Figs. 4 displays the obtained group delay GD, transmission loss S_{21}, and return loss S_{11}.

As highlighted in Fig. 4(a), by changing d_0 from 10 mm to 11 mm, it can be seen that the first and second center frequencies show a clear shift from 2.56 GHz to 2.33 GHz and 3.19 GHz to 2.91 GHz, respectively. The maximum delay varies less than 0.2 ns, S_{21} varies less than 0.1 dB, while S_{11} variation is less than 0.2 dB for the first and second center frequencies. Moreover, as depicted in Fig. 4(b) and Fig. 4(c), the multi coupler topology illustrates transmission coefficient better than 3 dB and reflection coefficient better than 15 dB.

2) PARAMETRIC ANALYSIS OF CL SPACE s

The CL effect was investigated by varying coupling space s from 3 mm to 4 mm during the S-parameter simulations.

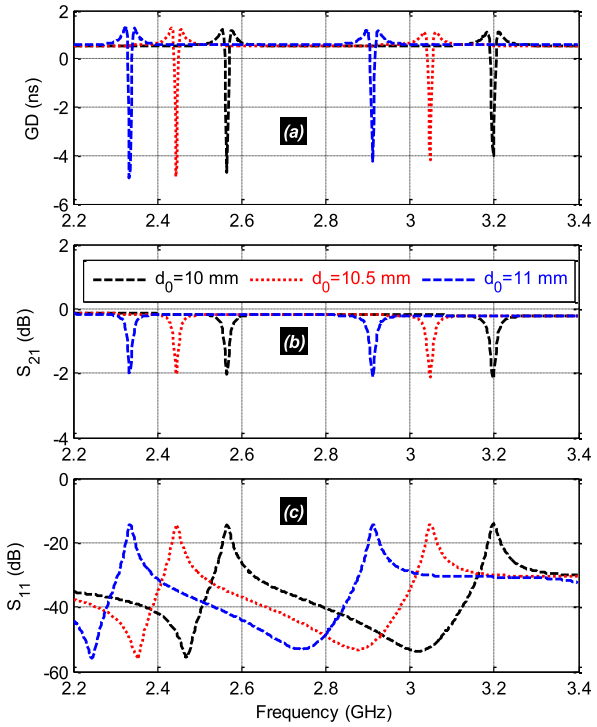

FIGURE 4. Parametric results analysis results versus d_0: (a) GD, (b) S_{21}, and (c) S_{11}.

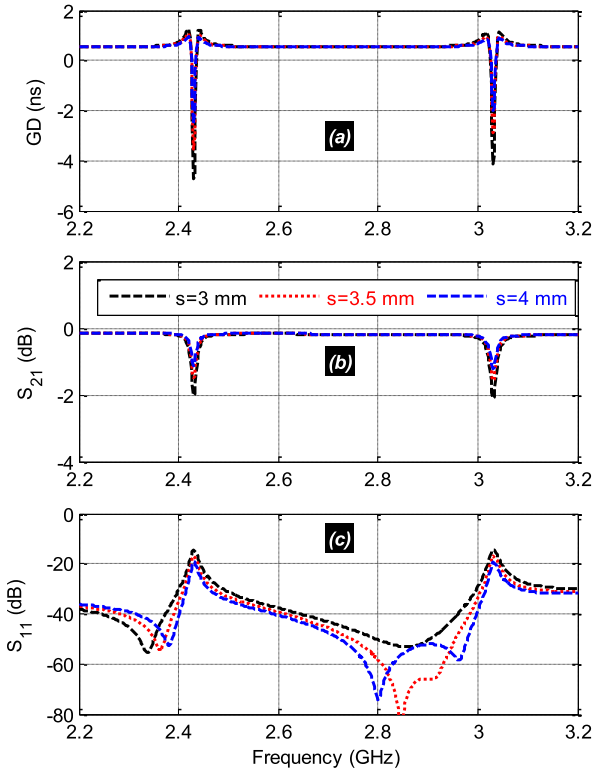

FIGURE 5. Parametric results analysis results versus s: (a) GD, (b) S_{21} and (c) S_{11}.

Figs. 5 display the obtained GD, S_{21} and S_{11} from 2.2 GHz to 3.2 GHz. As depicted in Fig. 5(a), the NGD first and second center frequencies are approximately 2.43 GHz

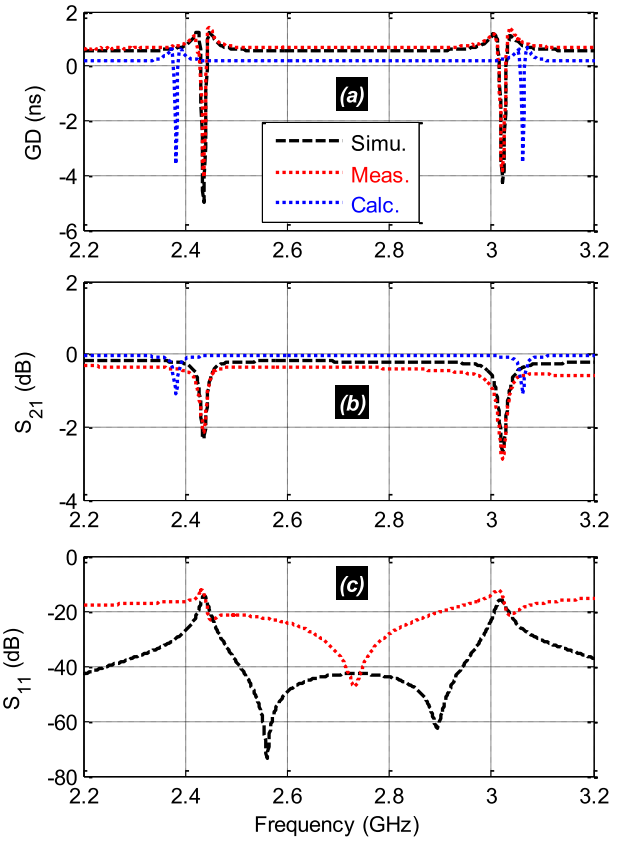

FIGURE 6. (a) Group delay, (b) transmission coefficient S_{21} and (c) Reflection coefficient S_{11} of the fabricated NGD circuit shown in Fig. 3(b).

and 3.03 GHz, which are insensitive to the variation of s. Within the considered variation range, the absolute value of NGD level decreases when s increases. Moreover, similar to the GD, in the considered range of s, S_{21} varies from −2 dB to −1.15 dB and −2.13 dB to −1.21 dB at the first and second center frequencies, respectively. S_{11} varies from −14.49 dB to −19.55 dB and −14.37 dB to −19.53 dB at the first and second center frequencies, respectively.

C. DISCUSSION ON THE DUAL-BAND NGD RESULTS OF THE TESTED MULTI-COUPLED LINE CIRCUIT

The experimental validation of the proposed NGD topology will be explored in the present subsection. Comparisons of results from theory, HFSS®simulation from ANSYS®, and measurements are discussed.

Similar to classical microwave circuits, the NGD tests, which are based on S-parameter analysis, were realized with a Vector Network Analyzer (VNA). The fabricated NGD prototype, previously introduced in Fig. 3(b), was measured with VNA Rohde & Schwarz (ZNB-20, frequency band 100 kHz to 20 GHz).

Comparisons between the theory, HFSS simulated ("Simu."), and measured ("Meas.") results have been carried out in the frequency band from 2.2 GHz to 3.2 GHz. The theory, simulated, and measured GDs and S-parameters are plotted in Figs. 6. It can be pointed out that these comparative

TABLE 2. The proposed circuit NGD specifications.

Validation Method	*Center frequency*	*GD (ns)*	*BW (MHz)*	S_{21} *(dB)*	S_{11} *(dB)*
Simu.	f_1=2.436 GHz	-5	12	-2.2	-12
	f_2=3.022 GHz	-4.2	13	-2.8	-14.02
Meas.	f_1=2.436 GHz	-4.06	12	-2.13	-12.61
	f_2=3.022 GHz	-3.83	13	-2.86	-12.40
Calc.	f_1=2.382 GHz	-3.55	10	-1.08	-
	f_2=3.062 GHz	-3.60	10	-1.08	-

results present a very good agreement. As expected, in the working frequency band, the tested prototype behaves as a bandpass NGD behaviors around first and second center frequencies of approximately $f_1 = 2.43$ GHz and $f_2 = 3.02$ GHz.

Table 2 summarizes the differences between theory, simulated, and measured NGD parameters. Figs. 6 illustrates the good performances of the multi coupler NGD topology in terms of group delay, transmission coefficient, and reflection coefficient at f_1 and f_2. As depicted in Fig. 6(a), the tested NGD circuit has NGD of approximately -4.06 ns over 12 MHz bandwidth at f_1 and has NGD of approximately -3.83 ns over 13 MHz bandwidth at f_2. It can be seen from Fig. 6(b) and 6(c) that in the test frequency band, S_{21} and S_{11} are globally better than -3 dB and -12 dB, respectively. The frequency shift, between the theory, simulation, and measurement results are mainly due to the dielectric substrate effective permittivity dispersion and the right-angles connection between TL and CLs. The theory results neglect the influence of these two factors, but the influences are included in HFSS simulation and test results. The slight difference in NGD, S_{21}, and S_{11} values are mainly due to fabrication inaccuracies, dielectric substrate effective permittivity, and losses versus the aided computational method accuracy.

D. DISCUSSION ON THE PERFORMANCE OF THE PROPOSED NGD CIRCUIT

The basic performance comparative results between the proposed NGD topology and the existing ones available in the literature [37]–[39] are summarized in Table 3. The introduced NGD topology presents the following advantages:

- Considerable fully distributed elements without lossy lumped component,
- Low signal attenuation, which is less than 2.86 dB,
- A reflection coefficient better than -12 dB and without the need for external matching networks in the NGD bandwidth.

TABLE 3. Performance comparison.

Ref.	f (GHz)	*GD* (ns)	S_{21}(dB)	S_{11}(dB)	*FOM*
[39]	f_1=2.14	-3	-34.2	-17	0.0150
	f_2=3.5	-3.1	-34.9	-17	0.0100
[40]	f_1=3.5	-4.54	-47.4	-	0.0023
	f_2=5.15	-4.2	-38.8	-	0.0048
[41]	f_1=0.667	-1.19	-18.2	-24.8	0.0338
	f_2=1.377	-1.19	-18.2	-24.7	0.0332
This work	f_1=2.436	-4.06	-2.13	-12.61	0.0381
	f_2=3.022	-3.83	-2.86	-12.40	0.0358

The designed NGD has a better NGD performance and FOM, which is defined in [39] as

$$FOM = |GD(f_0)| \times BW \times |S_{21}(f_0)| \tag{27}$$

It is noteworthy that the NGD frequencies are limited by:

- The substrate dispersions which are defined by the manufacturers,
- And the fabrication accuracies of the TL physical sizes and spaces.

V. CONCLUSION

An innovative analytical design of low-loss dual-band NGD circuit is investigated. The NGD topology consisting of two CLs and three TLs with different length is proposed. The difference in the physical length of the three TLs is used to generate the dual-band NGD phenomenon. By combining the CL and TL theories, the circuit's S-parameters and group delay model can be developed. It is analytically certificated that this novel circuit can be susceptible to generate the NGD phenomenon.

To confirm the feasibility of the NGD analytical design, a microstrip prototype of the multi-CL circuit topology was designed, simulated, fabricated, and measured. As expected, the measured results highlight the dual-band NGD behavior. It was shown that the tested prototype generates the dual-band NGD phenomenon with minimal values better than -4 ns and -3.8ns around the first and second center frequencies, respectively. As expected, the theory and measurement and simulation results were found to be in very good correlation. The NGD circuits respect satisfy all the criteria of RF/microwave circuits. Compared to the most of existing dual band NGD topologies [37]–[39], the proposed one presents huge advantages in low transmission coefficient and using fully distributed elements without extra lumped components. The topology can also be potentially used for multi-band NGD function.

REFERENCES

[1] S. Lucyszyn, I. D. Robertson, and A. H. Aghvami, "Negative group delay synthesiser," *Electron. Lett.*, vol. 29, no. 9, pp. 798–800, Apr. 1993.

[2] G. V. Eleftheriades, O. Siddiqui, and A. K. Iyer, "Transmission line models for negative refractive index media and associated implementations without excess resonators," *IEEE Microw. Wireless Compon. Lett.*, vol. 13, no. 2, pp. 51–53, Feb. 2003.

[3] C. D. Broomfield and J. K. A. Everard, "Broadband negative group delay networks for compensation of microwave oscillators and filters," *Electron. Lett.*, vol. 36, no. 23, pp. 1931–1933, Nov. 2000.
[4] O. F. Siddiqui, M. Mojahedi, and G. V. Eleftheriades, "Periodically loaded transmission line with effective negative refractive index and negative group velocity," *IEEE Trans. Antennas Propag.*, vol. 51, no. 10, pp. 2619–2625, Oct. 2003.
[5] O. F. Siddiqui, S. J. Erickson, G. V. Eleftheriades, and M. Mojahedi, "Time-domain measurement of negative-index transmission-line metamaterials," *IEEE Trans. Microw. Theory Techn.*, vol. 52, no. 5, pp. 1449–1453, May 2004.
[6] Y. Jeong, H. Choi, and C. D. Kim, "Experimental verification for time advancement of negative group delay in RF electronic circuits," *Electron. Lett.*, vol. 46, no. 4, pp. 306–307, Feb. 2010.
[7] L. He, W. Li, J. Hu, and Y. Xu, "A 24-GHz source-degenerated tunable delay shifter with negative group delay compensation," *IEEE Microw. Wireless Compon. Lett.*, vol. 28, no. 8, pp. 687–689, Aug. 2018.
[8] B. Ravelo, M. Le Roy, and A. Pérennec, "Application of negative group delay active circuits to the design of broadband and constant phase shifters," *Microw. Opt. Technol. Lett.*, vol. 50, no. 12, pp. 3078–3080, Dec. 2008.
[9] B. Ravelo, A. Pérennec, and M. Le Roy, "Synthesis of frequency-independent phase shifters using negative group delay active circuit," *Int. J. RF Microw. Comput.-Aided Eng.*, vol. 21, no. 1, pp. 17–24, Jan. 2011.
[10] T. Eudes and B. Ravelo, "Cancellation of delays in the high-rate interconnects with UWB NGD active cells," *Appl. Phys. Res.*, vol. 3, no. 2, pp. 81–88, Nov. 2011.
[11] K.-P. Ahn, R. Ishikawa, and K. Honjo, "Group delay equalized UWB InGaP/GaAs HBT MMIC amplifier using negative group delay circuits," *IEEE Trans. Microw. Theory Techn.*, vol. 57, no. 9, pp. 2139–2147, Sep. 2009.
[12] S. K. Podilchak, B. M. Frank, A. P. Freundorfer, and Y. M. M. Antar, "High speed metamaterial-inspired negative group delay circuits in CMOS for delay equalization," in *Proc. 2nd Microsystems Nanoelectronics Res. Conf.*, Ottawa, ON, Canada, Oct. 2009, pp. 9–12.
[13] H. Noto, K. Yamauchi, M. Nakayama, and Y. Isota, "Negative group delay circuit for feed-forward amplifier," in *IEEE MTT-S Int. Microw. Symp. Dig.*, Honolulu, HI, USA, Jun. 2007, pp. 1103–1106.
[14] H. Choi, Y. Jeong, C. D. Kim, and J. S. Kenney, "Efficiency enhancement of feedforward amplifiers by employing a negative group-delay circuit," *IEEE Trans. Microw. Theory Techn.*, vol. 58, no. 5, pp. 1116–1125, May 2010.
[15] H. Choi, Y. Jeong, C. D. Kim, and J. S. Kenney, "Bandwidth enhancement of an analog feedback amplifier by employing a negative group delay circuit," *Prog. Electromagn. Res.*, vol. 105, pp. 253–272, 2010.
[16] H. Mirzaei and G. V. Eleftheriades, "Arbitrary-angle squint-free beamforming in series-fed antenna arrays using non-foster elements synthesized by negative-group-delay networks," *IEEE Trans. Antennas Propag.*, vol. 63, no. 5, pp. 1997–2010, May 2015.
[17] A. Taslimi, W. Alomar, and A. Mortazawi, "Phase compensated serially fed array using the antenna as a part of negative group delay circuit," in *IEEE MTT-S Int. Microw. Symp. Dig.*, May 2015, pp. 1–4.
[18] W. Alomar and A. Mortazawi, "Elimination of beam squint in uniformly excited serially fed antenna arrays using negative group delay circuits," in *Proc. IEEE Int. Symp. Antennas Propag.*, Chicago, IL, USA, Jul. 2012, pp. 1–2.
[19] H. Mirzaei and G. V. Eleftheriades, "Realizing non-Foster reactances using negative-group-delay networks and applications to antennas," in *Proc. IEEE Radio Wireless Symp. (RWS)*, Newport Beach, CA, USA, Jan. 2014, pp. 58–60.
[20] H. Mirzaei and G. V. Eleftheriades, "Realizing non-foster reactive elements using negative-group-delay networks," *IEEE Trans. Microw. Theory Techn.*, vol. 61, no. 12, pp. 4322–4332, Dec. 2013.
[21] T. Zhang, R. Xu, and C.-T.-M. Wu, "Unconditionally stable non-foster element using active transversal-filter-based negative group delay circuit," *IEEE Microw. Wireless Compon. Lett.*, vol. 27, no. 10, pp. 921–923, Oct. 2017.
[22] M. Zhu and C.-T. M. Wu, "A tunable non-foster T-network loaded transmission line using distributed amplifier-based reconfigurable negative group delay circuit," in *Proc. Asia–Pacific Microw. Conf. (APMC)*, Kyoto, Japan, Nov. 2018, pp. 720–722.
[23] H. Mirzaei and G. V. Eleftheriades, "Unilateral non-foster elements using loss-compensated negative-group-delay networks for guided-wave applications," in *IEEE MTT-S Int. Microw. Symp. Dig.*, Jun. 2013, pp. 1–4.
[24] F. Wan, L. Wang, Q. Ji, and B. Ravelo, "Canonical transfer function of band-pass NGD circuit," *IET Circuits, Devices Syst.*, vol. 13, no. 2, pp. 125–130, Mar. 2019.
[25] F. Wan, N. Li, B. Ravelo, J. Ge, and B. Li, "Time-domain experimentation of NGD ActiveRC-network cell," *IEEE Trans. Circuits Syst. II, Exp. Briefs*, vol. 66, no. 4, pp. 562–566, Apr. 2019.
[26] B. Ravelo, "On low-pass, high-pass, bandpass, and stop-band NGD RF passive circuits," *URSI Radio Sci. Bull.*, vol. 2017, no. 363, pp. 10–27, Dec. 2017.
[27] B. Ravelo, A. PÉrennec, M. L. Roy, and Y. G. Boucher, "Active microwave circuit with negative group delay," *IEEE Microw. Wireless Compon. Lett.*, vol. 17, no. 12, pp. 861–863, Dec. 2007.
[28] B. Ravelo, "Baseband NGD circuit with RF amplifier," *Electron. Lett.*, vol. 47, no. 13, pp. 752–754, Jun. 2011.
[29] B. Ravelo, "Synthesis of RF circuits with negative time delay by using LNA," *Adv. Electromagn.*, vol. 2, no. 1, pp. 44–54, Feb. 2013.
[30] F. Wan, N. Li, B. Ravelo, Q. Ji, B. Li, and J. Ge, "The design method of the active negative group delay circuits based on a microwave amplifier and an RL-series network," *IEEE Access*, vol. 6, pp. 33849–33858, 2018.
[31] T. Shao, Z. Wang, S. Fang, H. Liu, and S. Fu, "A compact transmission-line self-matched negative group delay microwave circuit," *IEEE Access*, vol. 5, pp. 22836–22843, 2017.
[32] F. Wan, L. Wu, B. Ravelo, and J. Ge, "Analysis of interconnect line coupled with a radial-stub terminated negative group delay circuit," *IEEE Trans. Electromagn. Compat.*, early access, Aug. 30, 2019, doi: 10.1109/TEMC.2019.2936266.
[33] F. Wan, N. Li, B. Ravelo, Q. Ji, and J. Ge, "S-parameter model of three parallel interconnect lines generating negative group-delay effect," *IEEE Access*, vol. 6, pp. 57152–57159, 2018.
[34] Z. Wang, Y. Cao, T. Shao, S. Fang, and Y. Liu, "A negative group delay microwave circuit based on signal interference techniques," *IEEE Microw. Wireless Compon. Lett.*, vol. 28, no. 4, pp. 290–292, Apr. 2018.
[35] G. Chaudhary and Y. Jeong, "Low signal-attenuation negative group-delay network topologies using coupled lines," *IEEE Trans. Microw. Theory Techn.*, vol. 62, no. 10, pp. 2316–2324, Oct. 2014.
[36] H. Choi, Y. Kim, Y. Jeong, and C. D. Kim, "Synthesis of reflection type negative group delay circuit using transmission line resonator," in *Proc. 39th Eur. Microw. Conf.*, Sep. 2009, pp. 605–902.
[37] H. Choi, Y. Jeong, J. Lim, S.-Y. Eom, and Y.-B. Jung, "A novel design for a dual-band negative group delay circuit," *IEEE Microw. Wireless Compon. Lett.*, vol. 21, no. 1, pp. 19–21, Jan. 2011.
[38] G. Chaudhary, Y. Jeong, and J. Lim, "Miniaturized dual-band negative group delay circuit using dual-plane defected structures," *IEEE Microw. Wireless Compon. Lett.*, vol. 24, no. 8, pp. 521–523, Aug. 2014.
[39] T. Shao, S. Fang, Z. Wang, and H. Liu, "A compact dual-band negative group delay microwave circuit," *Radioengineering*, vol. 27, no. 4, pp. 1070–1076, Sep. 2018.
[40] B. Ravelo and S. De Blasi, "An FET-based microwave active circuit with dual-band negative group delay," *J. Microw., Optoelectron. Electromagn. Appl.*, vol. 10, no. 2, pp. 355–366, Dec. 2011.
[41] Y. Meng, Z. Wang, S. Fang, T. Shao, H. Liu, and Z. Chen, "Dual-band negative group delay microwave circuit with low signal attenuation and arbitrary frequency ratio," *IEEE Access*, vol. 8, pp. 49908–49919, 2020.